

Modelling vertical displacements due to hydrological load at stations of the Geocentric Reference System for the Americas (SIRGAS)

Claudio Brunini^{1,2,3}, Laura Sánchez⁴, Romina Galván^{2,3}, Herman Drewes⁵, Mauricio Gendè^{2,3}

(1) Argentinean - German Geodetic Observatory (Argentina); (2) Consejo Nacional de Investigaciones Científicas y Técnicas (Argentina); (3) Facultad de Ciencias Astronómicas y Geofísicas, Universidad Nacional de La Plata (Argentina); (4) Deutsches Geodätisches Forschungsinstitut, Technische Universität München (Germany); (5) Technische Universität München (Germany)

Abstract

This study concentrates on modelling seasonal vertical motions caused by variations of the hydrological load at geometrical reference frame stations. The proposed model relates the response of the Earth's crust (as measured by GNSS) to the hydrological load (inferred from GRACE). It is based on a numerical solution of the static equilibrium equation for an elastic medium (i.e. the Earth's crust) characterized by an elastic parameter. The elastic parameter relies on the combination of Poisson's ratio and Young's modulus. The empirical experiments combine (a) the normal equation systems (NEQ) calculated on a weekly basis for the SIRGAS reference frame along five years, with (b) monthly grids of equivalent water height (EWH) derived from GRACE for the same time span. The solution of the combined NEQ leads to the common adjustment of seven parameters per GNSS station; namely, three position coordinates at a certain epoch, three constant velocity coordinates, and one elastic parameter. The vertical positions predicted after the adjustment agree with the SIRGAS weekly positions within ± 3 mm at the one sigma level. This is interpreted as a first satisfactory evaluation of the capability of this method.

1 Introduction

1.1 SIRGAS realisation

This investigation is based on a time series of weekly GNSS-based loosely constrained NEQ for the SIRGAS network:

$$\mathbf{N}_w \cdot \mathbf{x}_w = \mathbf{b}_w \text{ with } \mathbf{N}_w = \mathbf{A}_w^T \mathbf{P}_w \mathbf{A}_w; \mathbf{b}_w = \mathbf{A}_w^T \mathbf{P}_w \mathbf{l}_w \quad \text{Eq. (1)}$$

\mathbf{A} is the design matrix; \mathbf{x} is the vector of parameters; \mathbf{l} is the observation vector; \mathbf{P} is the weighting matrix; and w stands for a week ($w = 1 \dots N_w$). Loosely constrained means that the geometry of the network is fully consistent with the GNSS orbits, but the network origin and orientation are loosely defined. These weekly loosely constrained NEQ are usually accumulated (Eq. (2)) to compute a multi-year realization under the premise of constant station velocities (Eq. (3)):

$$\left| \begin{array}{c} \sum_w (\mathbf{N}_w + \mathbf{P}_w) \\ \sum_w (t_w - t_0) \cdot \mathbf{N}_w \\ \sum_w (t_w - t_0)^2 \cdot \mathbf{N}_w \end{array} \right| \times \left| \begin{array}{c} \mathbf{x}_0 \\ \dot{\mathbf{x}} \end{array} \right| = \left| \begin{array}{c} \sum_w \mathbf{b}_w \\ \sum_w (t_w - t_0) \cdot \mathbf{b}_w \\ \sum_w (t_w - t_0)^2 \cdot \mathbf{b}_w \end{array} \right| \quad \text{Eq. (2)}$$

$$\mathbf{x}_w = \mathbf{x}_0 + \dot{\mathbf{x}}(t_w - t_0) \quad \text{Eq. (3)}$$

Non-linear motions are neglected for both, loosely constrained and fiducial stations, and they go hence into the residuals of the weekly positions with respect to the multi-year solution.

1.2 Vertical deformation attributed to hydrology

In this study, we assume that the vertical displacements of the SIRGAS stations are the elastic response of the Earth's crust to the seasonally changing load. Although gravity changes over the surface are due to atmospheric, non-tidal ocean and hydrological mass variations, in this region the hydrological contribution holds the main role of the overall contributions. Given an elastic planar half-space, the deformation caused by a pressure distribution (p) exerted in a region S around a point (i) can be described in the East (e), North (n), and vertical (v) directions as:

$$u = \frac{1}{4 \cdot \pi} \cdot \frac{1}{\lambda + \mu} \cdot \frac{\partial \chi}{\partial e} \quad \text{Eq. (4)} \quad v = \frac{1}{4 \cdot \pi} \cdot \frac{1}{\lambda + \mu} \cdot \frac{\partial \chi}{\partial n} \quad \text{Eq. (5)}$$

$$w = \frac{-1}{4 \cdot \pi \cdot \mu} \cdot \frac{\lambda + 2\mu}{\lambda + \mu} \cdot g \quad \text{Eq. (6)}$$

λ and μ are the Lamé parameters. χ and g are the Boussinesq logarithmic potential and the Newtonian potential, respectively:

$$\chi = \int_S p \cdot \log(r) \cdot ds \quad \text{Eq. (7)} \quad g = \int_S \frac{p}{r} \cdot ds \quad \text{Eq. (8)}$$

In the following, horizontal deformations and other loading sources than the hydrological are neglected. Under these conditions, from Eq. [6] and [8], we can write:

$$w = \frac{1 - \nu^2}{\pi \cdot E} \cdot \int_S \frac{g \cdot \rho \cdot h_w}{r} \cdot ds \quad \text{Eq. (9)}$$

In Eq. (9), h_w is the EWH distribution within the region S , ρ is the water density, g is the gravity acceleration and μ and E are Poisson's ratio and Young's modulus (which are mathematically related to the Lamé parameters). In this case, Young's modulus corresponds to the mean value within the region S where the integral is extended.

2 Modification of the GNSS-based NEQ system to account for the vertical load deformation

The NEQs in Eq. (1) are transformed from geocentric (X, Y, Z) to local (n, e, v) coordinates and the velocity in Eq. (3) for each station i ($i = 1 \dots N_i$) is replaced by:

$$n_{iw} = n_{i0} + \dot{n}_i \cdot (t_w - t_0) \quad \text{Eq. (10a)} \quad e_{iw} = e_{i0} + \dot{e}_i \cdot (t_w - t_0) \quad \text{Eq. (10b)}$$

$$v_{iw} = v_{i0} + \dot{v}_i \cdot (t_w - t_0) + \frac{1 - \nu^2}{\pi \cdot E_i} \cdot \int_S \frac{g \cdot \rho \cdot h_w}{r} \cdot ds \quad \text{Eq. (10c)}$$

The equation for the vertical component (Eq. (10c)) is linearized with respect to Young's modulus E :

$$v_{iw} - w_{iw0} = v_{i0} + \dot{v}_i \cdot (t_w - t_0) + \frac{w_{iw0}}{E_{i0}} \cdot \Delta E_i \quad \text{Eq. (11)}$$

E_{i0} is an a-priori value for Young's modulus at the station i ; w_{iw0} is the corresponding a-priori vertical deformation in the week w at that station:

$$w_{iw0} = \frac{1 - \nu^2}{\pi \cdot E_i} \cdot \int_S \frac{g \cdot \rho \cdot h_w}{r} \cdot ds \quad \text{Eq. (12)}$$

and $\Delta E_i = E_i - E_{i0}$ is the correction to the a-priori value of Young's modulus that is to be estimated within the solution of the NEQ. With the model stated by Eq. (10), (11) and (12), the accumulated NEQs (Eq. (2)) become:

$$\left| \begin{array}{c} \sum_w (\mathbf{N}_w + \mathbf{P}_w) \\ \sum_w (t_w - t_0) \cdot \mathbf{N}_w \\ \sum_w (t_w - t_0)^2 \cdot \mathbf{N}_w \\ \sum_w (\mathbf{W}_{w0} \bullet / \mathbf{E}_0)^T \cdot \mathbf{N}_w \cdot (\mathbf{W}_{w0} \bullet / \mathbf{E}_0) \end{array} \right| \times \left| \begin{array}{c} \mathbf{x}_0 \\ \dot{\mathbf{x}} \\ \Delta E \end{array} \right| = \left| \begin{array}{c} \sum_w (\mathbf{b}_w - \mathbf{W}_{w0}) \\ \sum_w (t_w - t_0) \cdot (\mathbf{b}_w - \mathbf{W}_{w0}) \\ \sum_w (\mathbf{W}_{w0} \bullet / \mathbf{E}_0)^T \cdot (\mathbf{b}_w - \mathbf{W}_{w0}) \end{array} \right| \quad \text{Eq. (13)}$$

\bullet and the upper index $[\bullet]$ denote the right array division and the use of local (n, e, v) coordinates, respectively. The a-priori value for Young's modulus at the different stations is inferred from the seismic velocities and the crustal densities provided by the model CRUST-1 (Fig. 1). As integration region (S_i in Eq. (9)), a circle of 7.5° around each station is selected.

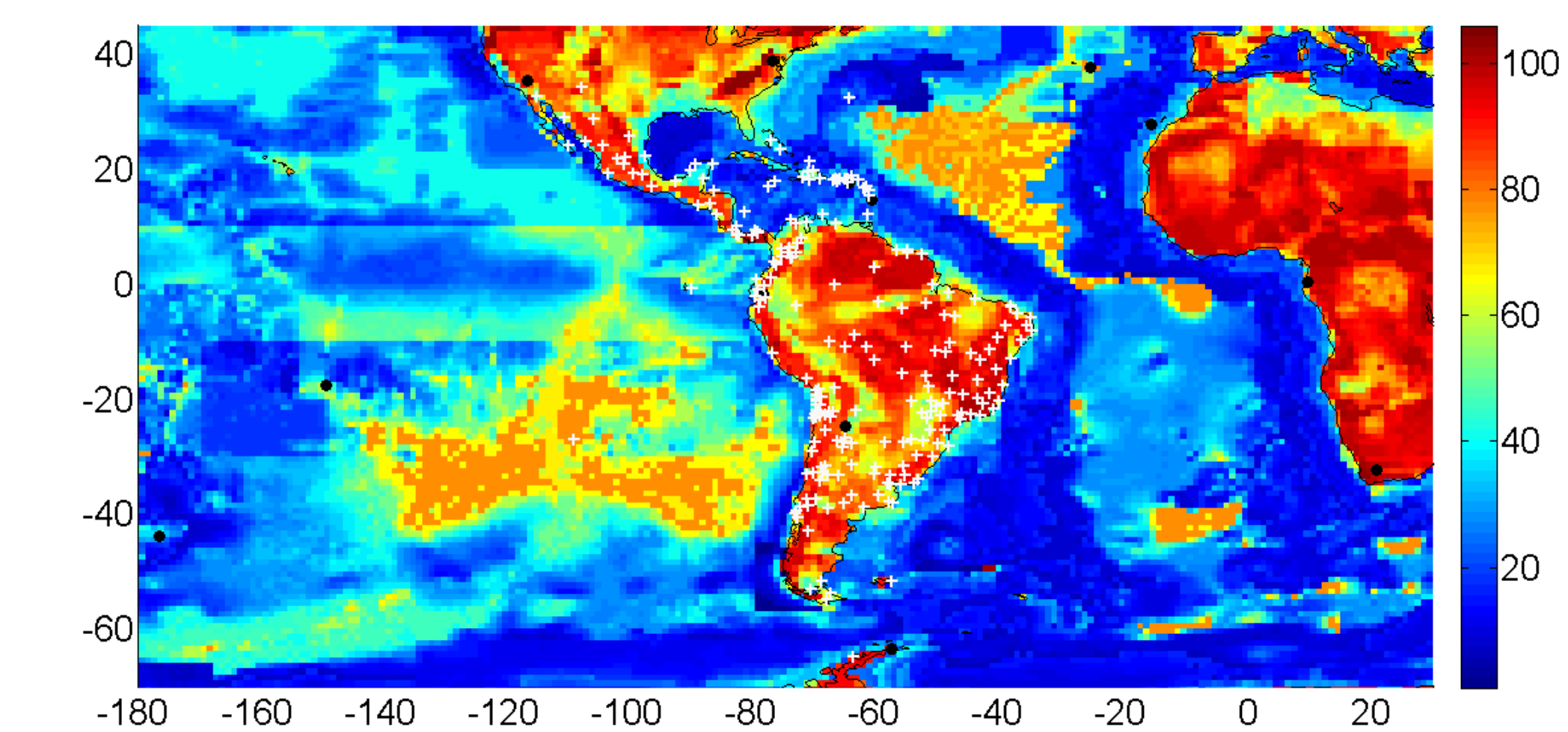


Fig. 1: 1°x1°-grid with a-priori values for Young's modulus [GPa]. Black dots represent the fiducial stations used to solve the NEQs and the white crosses represent the SIRGAS stations.

Monthly mean grids of $0.25^\circ \times 0.25^\circ$ of EWH are derived from CSR Release-05 GRACE Level-2 data products following the computational scheme presented in Fig. (2). The weekly EWH required to evaluate the integral in Eq. (12) are obtained by cubic interpolations of the four adjacent monthly mean values.

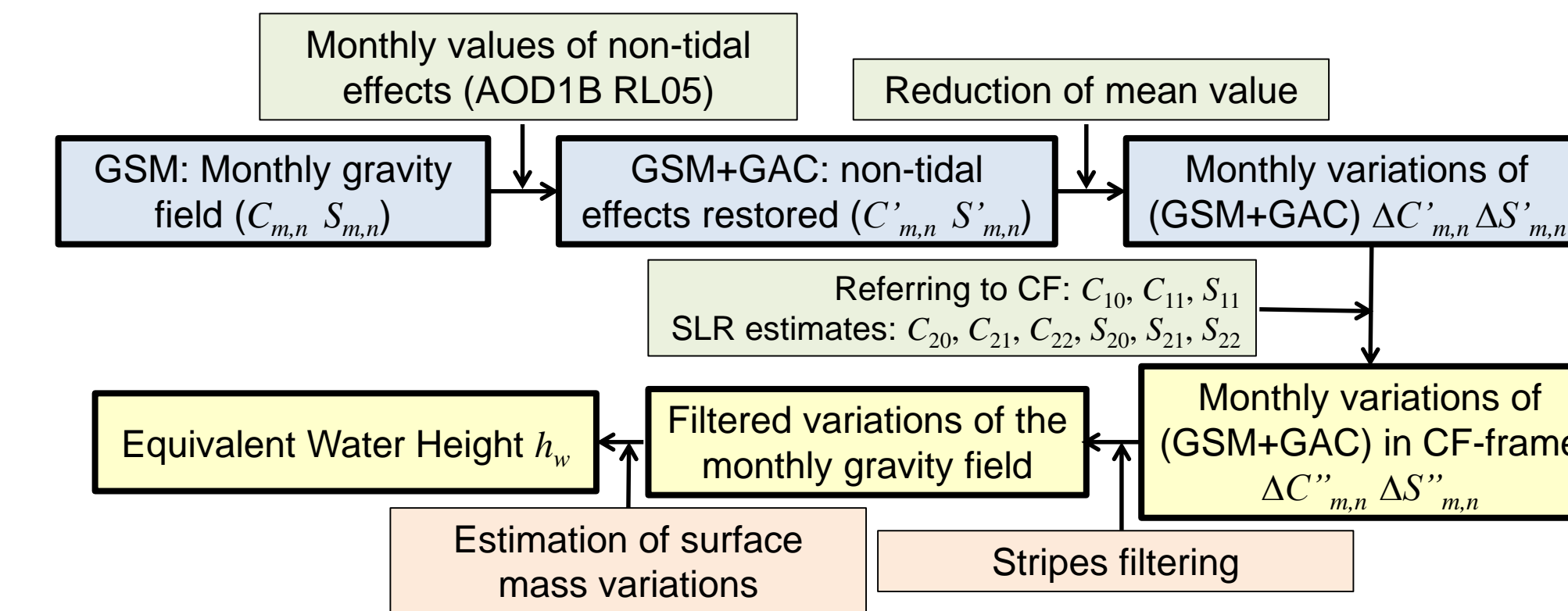


Fig. 2: Assessment of EWH values from monthly GRACE global gravity field time series (GSM): Mean values of AOD1B (Atmosphere and Ocean De-aliasing level-1B) are restored to take into account loading deformation caused by those effects. Degree one coefficients are considered to refer the GSM to the centre of figure (CF) and the degree two coefficients are replaced with satellite laser ranging (SLR)-based estimates.

3 Results

The empirical experiments are based on the analysis of 265 weeks (from 2010.3 to 2015.4) and 254 stations (Fig. 1). All the stations accumulate two or more years of data without anomalies (e.g. seismic jumps, post-seismic relaxation, unhandled antenna change, etc.). Stations are grouped according to the influence of the hydrological signal on the variation of their vertical positions. The classification criteria are:

- The magnitude of the vertical displacement assessed by $D_i = STD(rx_{iw})$. rx_{iw} represents the residuals of the weekly station vertical positions with respect to the constant velocities;
 - The correlation between the station displacements and the hydrological signal assessed by $r_i = COR(rx_{iw}, rw_{iw})$. rw_{iw} denotes the residuals of the hydrological displacement predicted using Eq. (12) with respect to a linear fit.
- Based on these quantities, the following grouping is established (Fig. 3):
- $D_i \uparrow r_i \uparrow$ ($D_i \geq 0.005$ m, $r_i \geq 0.5$): stations with great vertical deformation highly correlated with the hydrological signal;
 - $D_i \uparrow r_i \downarrow$ ($D_i \geq 0.005$ m, $r_i < 0.5$): stations with great vertical deformation not correlated with the hydrological signal;
 - $D_i \downarrow r_i \downarrow$ ($D_i < 0.005$ m, $r_i \geq 0.5$): stations with small vertical deformation not correlated with the hydrological signal;
 - $D_i \downarrow r_i \uparrow$ ($D_i < 0.005$ m, $r_i < 0.5$): stations with small vertical deformation highly correlated with the hydrological signal.

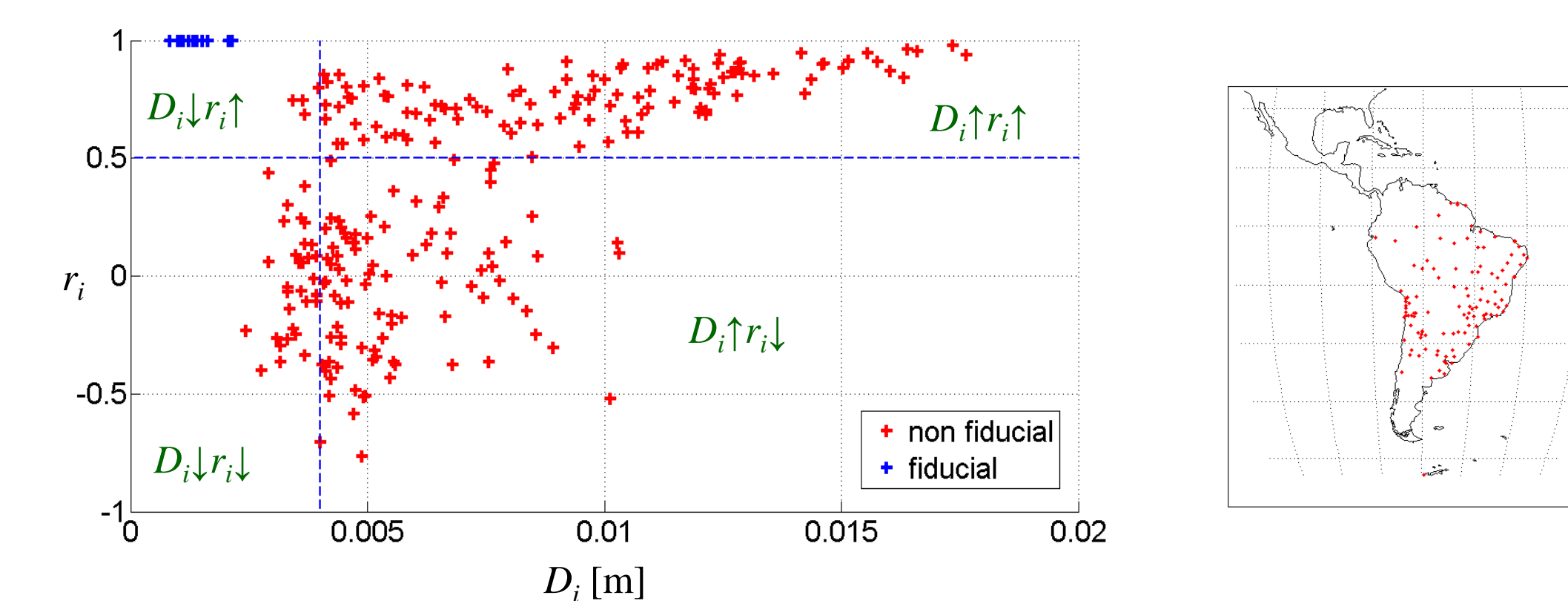


Fig. 3: Left side: influence of the hydrological signal on the variation of the vertical positions (blue crosses for the fiducials); right side: distribution of the stations with D_i, r_i .

Fig. 4 to 6 show the time series of weekly GNSS-based vertical positions (red crosses) at selected SIRGAS stations and the corresponding values predicted with Eq. (10c) after solving Eq. (13) for $\mathbf{x}_0, \dot{\mathbf{x}}, \Delta E$ (blue circles).

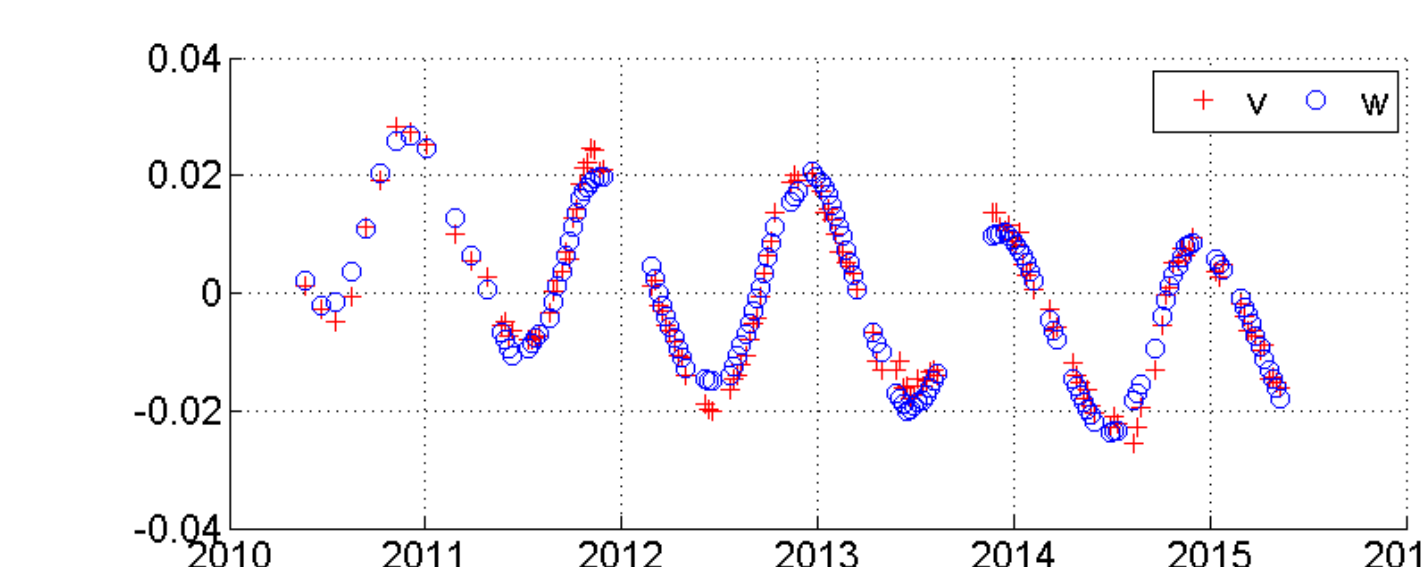


Fig. 4: GNSS-based (red crosses) and modelled (blue circles) vertical displacements in [m] at the SIRGAS station in Manaus, Brazil. It presents a large vertical deformation highly correlated with the hydrological signal (D_i, r_i).

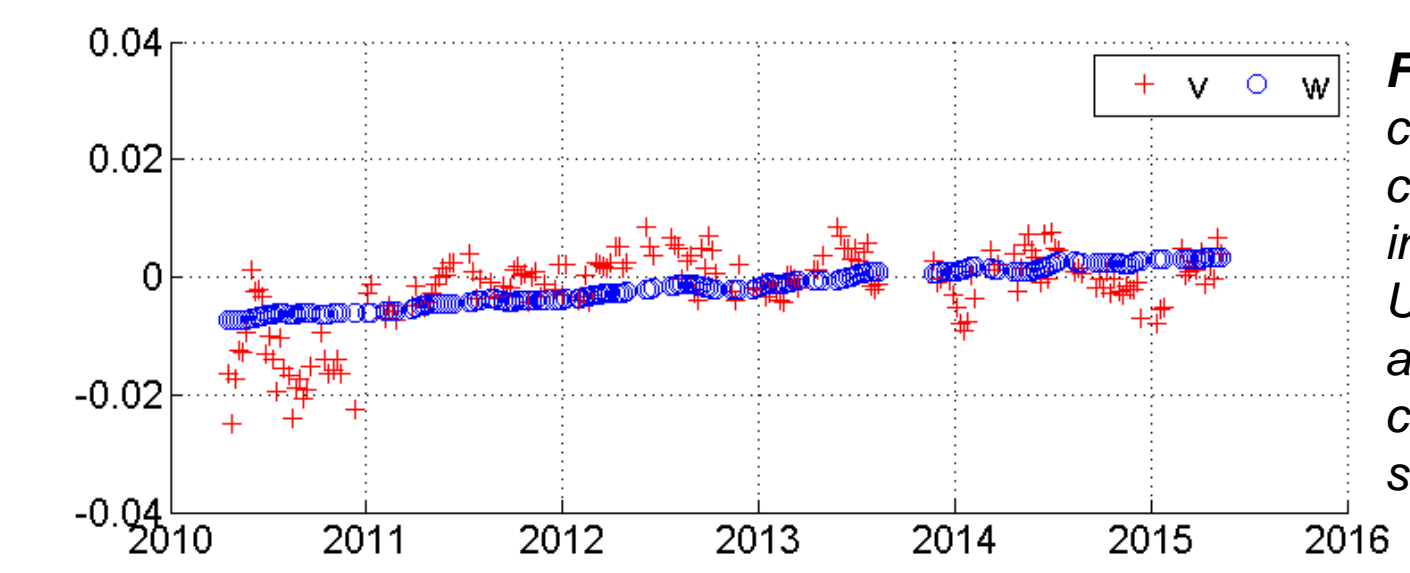


Fig. 5: GNSS-based (red crosses) and modelled (blue circles) vertical displacements in [m] at the SIRGAS station in Ushuaia, Argentina. It presents a large vertical deformation not correlated with the hydrological signal (D_i, r_i).

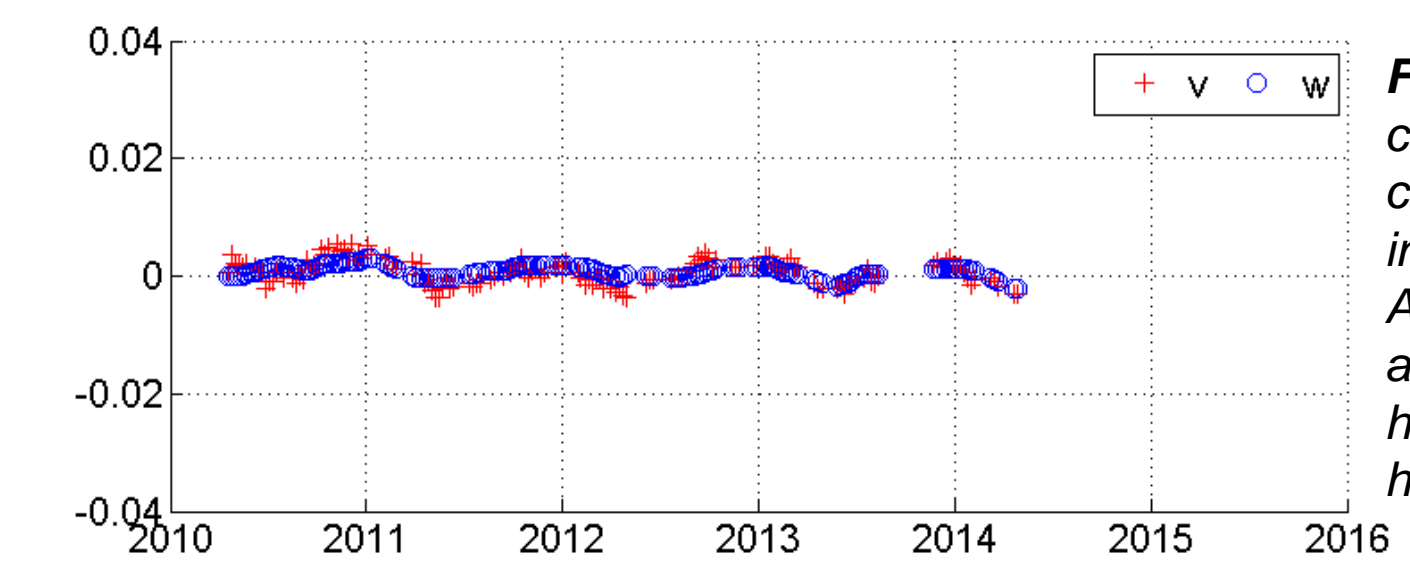


Fig. 6: GNSS-based (red crosses) and modelled (blue circles) vertical displacements in [m] at the SIRGAS station in Antofagasta, Chile. It presents a small vertical deformation highly correlated with the hydrological signal (D_i, r_i).

4 Closing remarks

The comparison of the predicted vertical positions using the model described by Eq. (4) to Eq. (13) with the GNSS-based vertical positions estimated within the SIRGAS reference frame analysis are around ± 3 mm at the one sigma level (Fig. 7). The main advantage of this strategy is the simultaneous estimation of the station coordinates (position and velocity) with an elastic parameter representing the transient deformation at the geodetic stations caused by the hydrological load (Fig. 8). As the method is based on global models, it may be applied in any region worldwide. The reliability of the obtained results is encouraging and suggests the possibility of improvements by refining the geophysical models and the algorithm for the accumulation of normal equations.

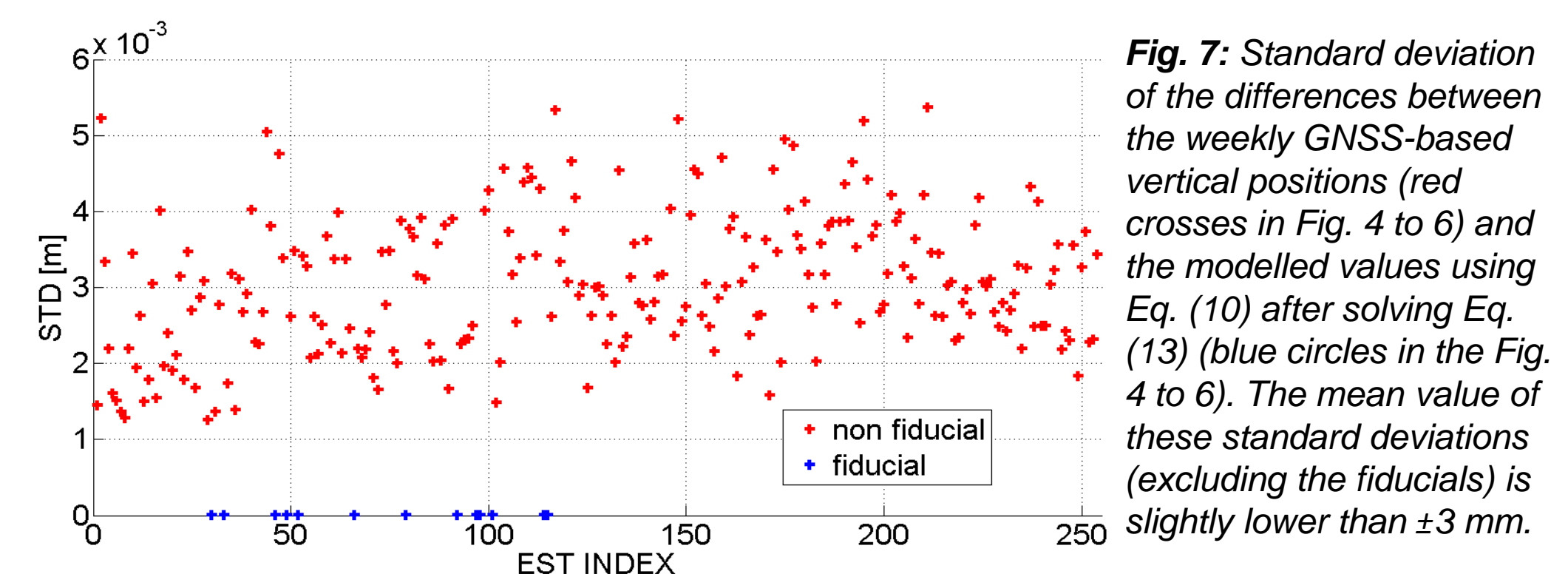


Fig. 7: Standard deviation of the differences between the weekly GNSS-based vertical positions (red crosses in Fig. 4 to 6) and the modelled values using Eq. (10) after solving Eq. (13) (blue circles in the Fig. 4 to 6). The mean value of these standard deviations (excluding the fiducials) is slightly lower than ± 3 mm.

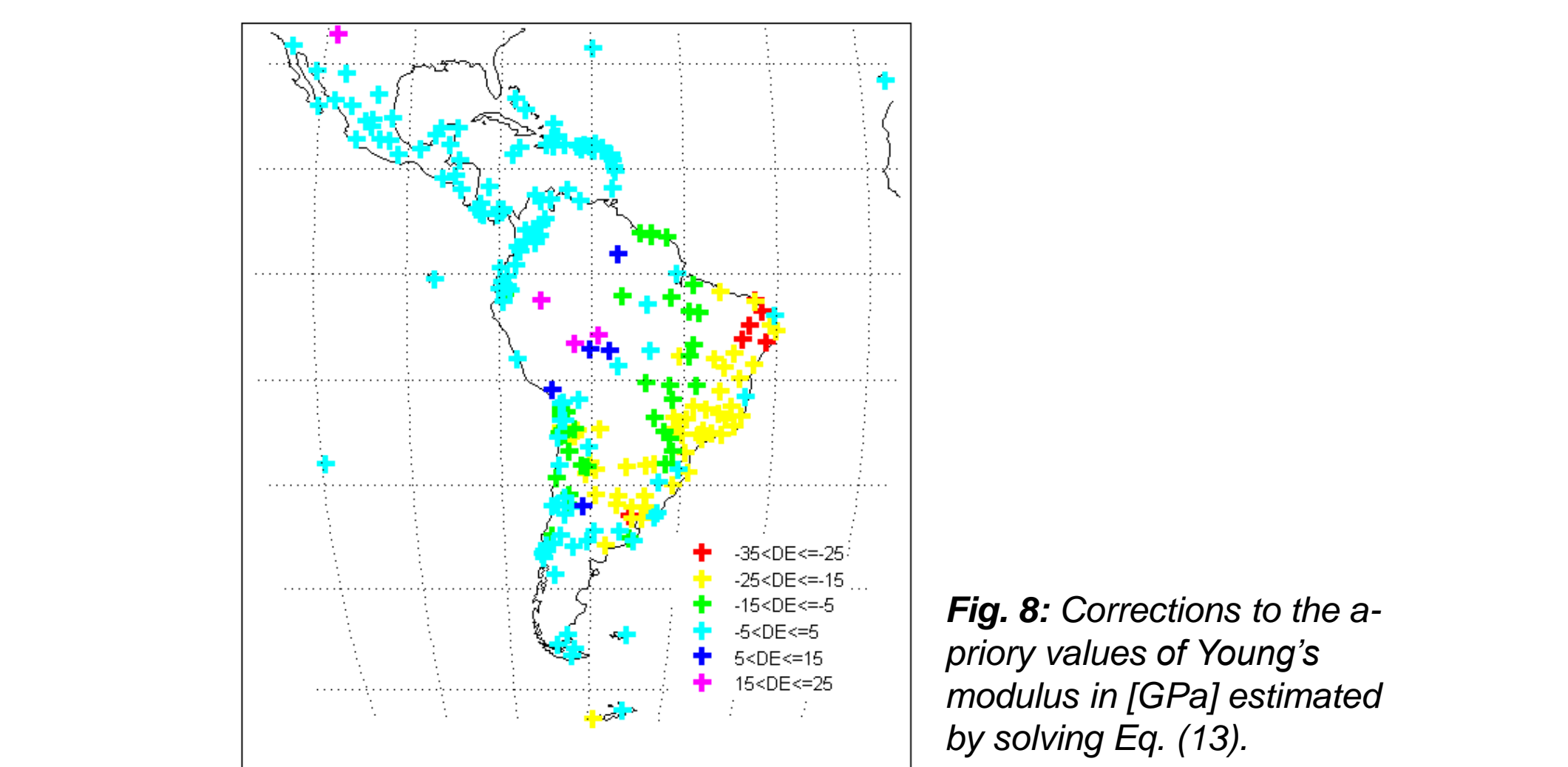


Fig. 8: Corrections to the a-priori values of Young's modulus in [GPa] estimated by solving Eq. (13).

Further reading

- Boussinesq J (1885) Application des Potentiels à l'Étude de l'Équilibre et du Mouvement des Solides Élastiques, p. 508, Gauthier-Villars, Paris.
- Galván R, Gendè M, Brunini C (2016) Regional model to estimate vertical deformations due to loading seasonal changes, IAG Symposia, 1001-110, 10.1007/1345_2015_101.
- Sánchez L, Drewes H, Brunini C, Mackern MV, Martínez W (2015) SIRGAS Core Network Stability, IAG Symposia, 10.1007/1345_2015_143.
- Sánchez L, Drewes H (2016) Crustal deformation and surface kinematics after the 2010 earthquakes in Latin America. J. Geodyn., 10.1016/j.jog.2016.06.005.
- Turcotte DL, Schubert G. (2002) Geodynamics, Cambridge University Press, 456 pp.
- Laske G, Masters G, Ma Z, Pasyanos M (2013) Update on CRUST1.0 - A 1-degree Global Model of Earth's Crust, Geophys. Res. Abstracts, 15, Abstract EGU2013-2658.